



1 **Large-scale ion generation for precipitation of atmospheric aerosols**

2

3 **Shaoxiang Ma¹, He Cheng¹, Jiacheng Li¹, Maoyuan Xu¹, Dawei Liu¹, and Kostya**

4 **Ostrikov²**

5

6 ¹State Key Lab of Advanced Electromagnetic Engineering and Technology, School of Electronic
7 and Electrical Engineering, Huazhong University of Science and Technology, WuHan, HuBei
8 430074, China

9 ²Institute for Future Environments and School of Chemistry and Physics, Queensland University of
10 Technology, Brisbane, Queensland 4000, Australia

12 **Correspondence:** Dawei Liu (liudw@hust.edu.cn)

13

14 **Abstract.** Artificial rain is explored as a remedy to climate change caused farmland drought and
15 bushfires. Increasing the ion density in the open air is an efficient way to generate charged nuclei
16 from atmospheric aerosols and induce precipitation or eliminate fog. Here we report on the
17 development of the large commercial installation scale atmospheric ion generator based on corona
18 plasma discharges, experimental monitoring and numerical modeling of the parameters and range of
19 the atmospheric ions, and application of the generated ions to produce charged aerosols and induce
20 precipitation at a scale of a large cloud chamber. The coverage area of the ions generated by the large
21 corona discharge installation with the 7.2 km long wire electrode and applied voltage of -90 kV is
22 studied under prevailing weather conditions including wind direction and speed. By synergizing over
23 300,000 localized corona discharge points, we demonstrate a substantial decrease of the decay of
24 ions compared to a single corona discharge point in the open air, leading to a large-scale (30 m×23
25 m×90 m) ion coverage. Once aerosols combine with the generated ions, charged nuclei are produced.



1 The higher wind speed has led to the larger areas covered by the plasma generated ions. The cloud
2 chamber experiments (relative humidity $130\pm 10\%$) suggest that the charged aerosols generated by
3 ions with the density of $\sim 10^4/\text{cm}^3$ can accelerate the settlement of moisture by 38%. These results
4 are promising for the development of large-scale installations for the effective localized control of
5 atmospheric phenomena.

6

7

8

9

10

11

12

13

14

15

16

17

18

19

20

21

22



1 1. Introduction

2 The water cycle and rainfall on the Earth are affected by the climate change, causing widespread
3 droughts around the world (Dai, 2013; Trenberth et al., 2014). Recently, more and more forest fires
4 happened in North America, Australia and China. Besides that, the lack of water in many parts of
5 Asia and Africa seriously influence the local agriculture, industry, and human health (Jolly et al.,
6 2015; Lesk et al., 2016). The artificial rain has been used widely in many countries to alleviate the
7 drought problems by enhancing precipitation. The artificial rain is commonly realized by dispersing
8 substances, such as silver iodide, dry ice and table salts, which act as cloud condensation nuclei and
9 alter the physico-chemical processes within the cloud.

10 It is well known that the ions generated by galactic cosmic rays in the atmosphere directly affect the
11 changes in cloudiness of the Earth (Carslaw et al., 2002; Pierce and Adams, 2009). The experiment
12 in the Wilson chamber suggested that ions generated by radioactive materials acted as condensation
13 nuclei under supersaturation conditions (Yang et al., 2018). Nielsen *et al.* found that the charged
14 nuclei could remain in the condensation phase even when the relative humidity is less than 100%
15 (Nielsen et al., 2011). This is why plasma- and laser-based techniques have been employed to
16 generate the charged nuclei in the open air to try to realize rain enhancement or, alternatively, fog
17 elimination (Henin et al., 2009; Khain et al., 2004; Tan et al., 2016).

18 Ideally, the effects (e.g., precipitation of atmospheric aerosols) of the plasma-based methods should
19 be delivered over the areas of small-to-medium-size farmlands. Indeed, it appears appealing to install,
20 for example, a large-scale corona plasma discharge system on top of a hill and distribute the
21 generated ions using the wind. Indeed, corona plasma discharges can release high-concentration ion
22 fluxes, which can not only be transported to a large area by the upwind slope airflow, but also
23 effectively interact with atmospheric aerosols thereby generating charged nuclei needed to induce or
24 enhance water precipitation in the areas along the downwind direction. However, there are
25 formidable science and technological challenges to implement it in practice. First, we are not aware
26 of any systematic experimental and theoretical studies on the generation efficiency of ions, the



1 coverage area of ions and effect of wind on the ion transport at the relevant scale of the atmospheric
2 ion generating installations. Second, the high efficiency of the ion generation in the laboratory does
3 not necessarily translate into a similar performance at a scale. One reason is destructive interference
4 of multiple corona discharges along the same plasma-generating wire, addressed in this work. Third,
5 there are no reliable estimates of the volumes where the ions are generated at concentrations that are
6 appropriate for atmospheric aerosol precipitation. Fourth, the reliable quantitative estimates of the
7 significance of the effects of plasma-generated ions on moisture precipitation under real-world
8 conditions are very limited, if available at all. Fifth, quantitative effects of the real-world wind on the
9 ion coverage at the large installation scale are eagerly anticipated by the community.

10 In this work, we address all the above issues and report on the coverage area of ions generated by a
11 large corona discharge system with the 7.2 km long wire electrode and applied voltage of -90 kV.
12 The vertical and horizontal distribution of the ions in the downwind are measured under realistic
13 weather conditions. The numerical models of the corona discharge and ion transport are developed.
14 The results of numerical modelling are consistent with the experiment results, and indicates that the
15 ions produced by the plasma discharge device may affect aerosol precipitation over large areas
16 depending on the direction and speed of the wind. The effects of the plasma generated ions on
17 moisture precipitation are studied experimentally at a scale of a large cloud chamber.

18 **2. Methods**

19 **2.1 Corona discharge installation and ion measurements**

20 The large corona discharge system employed in this study has the floor area $\sim 11304 \text{ m}^2$ (**Figure 1** (a)
21 and (b)). Six poles each with the height of 20 m supporting the 7.2 km long wire electrode are
22 erected vertically and arranged in a regular hexagon array. The wire electrodes are divided into two
23 layers, at the height of 20 m and 15 m, i.e., with 5 m separation between the layers. There are 10 wire
24 electrodes in each layer, and the horizontal distance between the wires is 50 cm to avoid the mutual
25 interference. The stainless-steel wire has six strands and a diameter of 1 mm. The high voltage DC



1 power supply is Technix 44-2015, which can monitor the output voltage and current value in real
2 time.

3 **Figure 1** (c) shows the satellite image of test zone. The hexagon shows the large-scale corona
4 discharge system. The red points show the locations of the ion density measurements. The hydrogen
5 balloon carrying the ion counter (Air Ion Counter) is used to measure the vertical (5 m – 50 m) and
6 horizontal (20 m – 50 m) ion density in the downwind. The horizontal distance between the
7 hydrogen balloon measurement and the wire electrode is 20 m to ensure the safety of the experiment.
8 The image of the corona discharge on the wire electrode is taken by digital camera Nikon D800 with
9 the exposure time of 2 s. The optical emission spectroscopy (OES) of the negative corona discharge
10 on the wire electrode with the applied voltage of -40 kV is measured by an optical spectrometer
11 (Ocean optics USB4000+).

12 2.2 Ion transport model

13 The 2D numerical model is used to study the distribution of ions within 1 m from the wire
14 electrode. The model used in this study extends the existing models (He et al., 2013; Liu et al., 2012,
15 2014a, 2014b) to model the relevant phenomena at the relevant scales. The model solves the
16 Poisson's equation and the transport equations for neutral and charged species as a function of time.
17 The number density of each species is obtained by solving the continuity equation. The electric field
18 is obtained by solving the Poisson's equation. The electron energy is calculated by the electron
19 energy conservation equation.

20 The transient advection diffusion reaction equation (equation (1)) is used to study the effect of wind
21 on the transport of ions (Albani et al., 2015; Ashrafi et al., 2017; Schleder and Martins, 2016)

$$22 \quad \frac{\partial c}{\partial t} + \mathbf{u} \nabla c = \nabla (\mathbf{K} \nabla c) - \lambda c, \quad c = c(\mathbf{x}, y, z, t) \quad , \quad (1)$$

23 where c is the crosswind-integrated concentration of ions, t is time, u is the wind speed, K is the eddy

24 diffusivity, ∇ is the position-gradient operator, $\nabla = \left(\frac{\partial}{\partial x}, \frac{\partial}{\partial y}, \frac{\partial}{\partial z} \right)$, and λ is the decay constant.



1 **2.3 Cloud chamber experiments**

2 The cloud chamber used to study the enhanced water condensation by ions has the size of 3 m×1.5
3 m×1.5 m (**Figure 2**). The temperature inside the chamber is 2±1°C during the experiment. The
4 dehumidifier (Gree DH40EF) and ultrasonic humidifier (Midea SC4E40) are used to control the
5 humidity supersaturation at 130±10%. The laser illuminator (YGL01, planar laser source) is used to
6 light up the cloud chamber. The changing process of droplets is recorded by the digital camera
7 (Nikon D800) with a microscopic lens. Finally, an acceptor with the cross section of 10 cm² is placed
8 at the bottom of the cloud chamber to accept the settlement of moisture.

9 **3. Results and discussion**

10 **3.1 Corona discharges and plasma characteristics**

11 The applied voltage on the wire electrode with the length of 7.2 km is -90 kV (**Figure 1**), and the
12 discharge current is 0.3 mA, so the plasma power is 27 W. **Figure 1** (e) shows that there are more
13 than 20 corona discharge points on the wire electrode with the length of 1 m. Because the distance
14 between the camera and the wire electrode is only 2 m, the applied voltage is therefore -40 kV to
15 ensure the experimental safety. Although the six strands of stranded stainless-steel wire have good
16 anti-stretching and anti-bending properties, there are numerous small peaks on the wires, which
17 help ignite corona discharges. Consequently, the minimum inception voltage of the corona discharge
18 on the wire is only -15 kV. More corona discharge points are thus expected for the field experiment
19 with the applied voltage of -90 kV.

20 **Figure 3** shows the OES data of the corona discharge on the wire electrode. The brightest peaks can
21 be seen around 315, 337, 350 and 380 nm, which are attributed to the nitrogen 2nd positive electronic
22 transition (N₂(C³Π_u - B³Π_g)) and its family of vibrational rotational level sub-transitions (Antao et al.,
23 2009; Hu et al., 2013; Wang et al., 2013; Zou et al., 2019). The OES of OH and O radicals are quite
24 low compared with N₂ species(Gan et al., 2019).



1 3.2 Ion transport

2 For the negative corona discharge, the plasma region only occupies a very small portion of the space
3 around the power electrode, negative ions occupy the region outside the plasma region (Chen and
4 Davidson, 2003; Riba et al., 2018; Yao et al., 2019; Zhang et al., 2019). **Figure 4** (c) shows the
5 boundary of the plasma region defined as the position where the reduced electric field of 80 Td is 0.1
6 cm from the electrode (Chen and Davidson, 2003). Therefore, the negative ion density at the
7 boundary of plasma region (~1cm from the electrode, reduced electric field ~10 Td) is chosen as the
8 source density of negative ions for each case.

9 As the applied voltage amplitude increases from 30 kV to 90 kV, the source density at 1 cm from the
10 single discharge point increases from $1.1 \times 10^8/\text{cm}^3$ to $3.9 \times 10^8/\text{cm}^3$, and the density at 1 m from the
11 single discharge point increased from $1.8 \times 10^6/\text{cm}^3$ to $8 \times 10^6/\text{cm}^3$ (**Figure 4** (b)). In addition, **Figure 4**
12 (a) suggests that the ion density in the whole simulation domain increases with the increasing applied
13 voltage amplitude.

14 **Figure 5** shows the effect of the wind on the transport of ions generated by a single corona discharge
15 point. The ion density at the plasma boundary is chosen as the source density. The ion density
16 measured at the position at 1 m from the electrode is consistent with the numerical result calculated
17 by Eq. (1). As the wind speed increases from 0 to 5.7 m/s, the ion density at 1 m increases from
18 $2.5 \times 10^6/\text{cm}^3$ to $4 \times 10^6/\text{cm}^3$, and the density at 3 m increases from $3.2 \times 10^4/\text{cm}^3$ to $2 \times 10^5/\text{cm}^3$, which
19 indicates that the diffusivity dominates the ions movement in the low electric field region, and the
20 wind convection can substantially enhance the ion transport (Albani and Albani, 2019; Ashrafi et al.,
21 2017; Hosseini and Stockie, 2016; Schleder and Martins, 2016).

22 **Figure 6** (a) shows the coverage range (horizontal/vertical (x/z) direction) of negative ions generated
23 by the large corona discharge system shown in **Figure 1**. In order to ensure the safety, the ion counter
24 carried by the balloon starts recording the negative ion density at the position of 20 m from the wire
25 electrode. The ion density decreases from $5 \times 10^5/\text{cm}^3$ to $8 \times 10^3/\text{cm}^3$ as the distance from the wire
26 electrode increases from 20m to 30m. Afterwards, the ion density decreases to the background value



1 as the horizontal distance increases to 40 m. The relatively high density $10^4/\text{cm}^3$ at the horizontal
2 position of 50 m can be attributed to the random enhanced transport by gusts. The width of the
3 coverage area in radial direction was 90 m. Therefore, the whole coverage volume was
4 approximately 30 m (long) \times 23 m (height) \times 90 m (width). Aerosols can combine with the ions
5 generated in this volume, thus creating a large number of charged nuclei within the volume (Anon,
6 2000; Bricard et al., 1968; Harrison, 2000; Harrison and Carslaw, 2003; Keefe et al., 1959).

7 It is interesting to note that the ion density at 20 m from the single corona discharge point is only
8 $10^2/\text{cm}^3$ (**Figure 6 (c)**), which is only 0.02% of the ion density generated by the large corona
9 discharge system (**Figure 6 (a)**). **Figure 1 (e)** suggests the presence of more than 45 corona discharge
10 points along the 1 m long wire electrode when the applied voltage is -40 kV, and the average distance
11 between corona discharge points is only 2.5 cm. For the large corona discharge system with the 7.2
12 km long wire electrode and applied voltage of -90 kV, the number of the corona discharge points is
13 expected to be at least 3.2×10^5 ($45 \times 7.2 \times 10^3$). The mutual interference was avoided by the horizontal
14 distance of 50 cm and the vertical distance of 5 m between the wires.

15 **Figure 6 (d)** shows the collective efficiency of ion transport of ions generated by the many corona
16 discharge points. Because the distance between the corona discharge points is in the cm range and
17 the coverage area of each corona discharge point is 25 m (x-direction) \times 30m (y-direction) (**Figure 6**
18 (c)), the overlap of the coverage areas results in the high ion density in the open air.

19 The comparison between the experimental (**Figure 6 (a)**) and simulation (**Figure 6 (c)**) results
20 suggest that the combination of numerous corona discharge points actually decreases the decay of
21 ions generated by a single corona discharge point in the open air, and substantially increases the
22 outward transport capacity of ions of the large corona discharge system. In the simulation model, by
23 decreasing the decay constant λ by 4.533 times, the equation (1) provides a similar coverage area as
24 measured in the experiment (compare **Figure 6 (a)** and (b)).

25 Because the large corona discharge system may be setup on the mountain top, e.g., with an altitude
26 of around 4,000 m (Farr and Chadwick, 2012; Mu et al., 2007; Shiyin et al., 2003; Zhou and Yang,



1 2010), the effect of the wind and applied voltage on the coverage area of large corona discharge
2 system is also studied by the numerical model.

3 **Figure 7** (a) – (c) suggest that as the wind speed increases from 2.89 m/s to 12.5 m/s, the axial length
4 of the coverage area (ion density $\sim 10^4/\text{cm}^3$) increases from 26 m to 73 m. **Figure 7** (d) – (f) suggests
5 that as the amplitude of the applied voltage increases from 60 kV to 180 kV, the axial length of the
6 coverage area increases from 34 m to 46 m. The comparison between the effects of the wind and
7 applied voltage indicates that the increasing transfer flux with the faster wind speed is a more
8 efficient way to increase the coverage area of the large corona discharge system. The larger coverage
9 area can facilitate the generation of charged nuclei, which eventually realize rain enhancement and
10 fog elimination (Frederick and Tinsley, 2018; Tinsley and Zhou, 2015; Zhang et al., 2018a).

11 **3.3 Ion-enhanced precipitation**

12 The cloud chamber is used to study the enhancement of droplets growth by ions before the
13 completion of the large-scale corona discharge system. The corona discharge on the needle electrode
14 (applied voltage of -23 kV) provides an environment with the ion density of $1.2 \times 10^5/\text{cm}^3 \sim$
15 $2 \times 10^4/\text{cm}^3$ in the cloud chamber, which corresponds to the ion density in the region 1 – 20 m from
16 the wire electrode (**Figure 6** (a)). The high ion density in the cloud chamber facilitates the aerosols
17 charging. Aerosols (diameter > 0.7) are mainly charged by the drift of ions on the electric field lines
18 intersecting the surface of aerosols. The diffusion of ions to the surface of aerosols also contribute to
19 the aerosols charging. (Jidenko and Borra, 2012)

20 The size distribution of droplets of the natural settling case and the ion-enhanced settling case are
21 compared in **Figure 8**. The droplet sizes are distributed mainly in the range of $10 \sim 40 \mu\text{m}$ for the
22 case of natural settling. The charged aerosols are generated through the combination of ions and
23 aerosols. Besides the conventional forces such as the thermophoretic and diffusophoretic forces, the
24 electric forces contribute to the collisions between the charged aerosols and uncharged aerosols.
25 (Cherrier et al., 2017; Hashino et al., 2014; Luan et al., 2019; Roy et al., 2019; Wang and Pruppacher,
26 1977; Zhang et al., 2018b; Zhang and Tinsley, 2017). The charged aerosols can induce the image



1 charge on uncharged aerosols, and the consequent electric forces are the short range attractive forces.
2 The previous simulation results suggest that the charged aerosols can increase the collision rate
3 between aerosols by 1 to 3 orders of magnitude.(Tan et al., 2016) Therefore, the droplet sizes are
4 distributed in the range of 50 - 80 μm for the case of charged aerosols settling case. However, the
5 uncharged aerosols of the natural settling case (control group) can only cause limited increase of the
6 particle size distribution. The large droplets generated by charged droplets can capture a large
7 number of small aerosols during their settling process and cause faster settling of supersaturated
8 water vapor in the cloud chamber. **Figure 8 (d)** indicates that the settling amount of moisture
9 induced by charged aerosols is 38% higher than in the natural settling case (control group) at 10 min
10 after the start of the experiment.

11 **3.4 Technoeconomic estimates**

12 As a simple techno-economic estimate, we note that the cost of the large corona discharge system
13 including the DC power supply, 6 poles, the wires with length of 7.2 km was less than 250,000
14 Chinese Yuan (CNY). The low-maintenance solar and wind power system (estimated cost of 50,000
15 CNY) can provide a continuous supply of renewable energy for the corona plasma discharge system.
16 This energy supply system can be installed on-site and operated off-the-grid. Even considering the
17 high construction cost of the system on the mid-altitude mountains to be about 200,000 CNY, the
18 total cost of the installation was approximately 500,000 CNY. Importantly, this cost is well below the
19 typical cost of a cloud seeding carried in China (at least 1 million CNY) to generate artificial rain.
20 After the completion of the setup and real-world testing and optimization of the large-scale corona
21 discharge installation, it may have an effect on the rainfall of downwind area. A similar approach can
22 be used for fog elimination applications, for example along the airport runways. Importantly, the
23 plasma system can be switched on to instantly generate the ions, and then switched off to also
24 instantly cease the ion production whenever the wind direction or other atmospheric conditions
25 change. This important feature of the plasma adds additional level of flexibility in commercial
26 operation of the system.



1 4. Conclusion and implications

2 To summarize, a large-scale corona plasma discharge system was installed to analyze the production
3 and the coverage area of negative ions that are capable to induce precipitation of atmospheric
4 aerosols in downwind direction. The nitrogen species dominated the optical emission spectra of the
5 negative corona discharges. The corona discharge was found to perform as a stable ion source with
6 the density of $\sim 10^8/\text{cm}^3$. The coverage area of the ions was dramatically improved by using over
7 300,000 corona discharge points, which also reduced the common destructive interference leading to
8 the decay of ion concentrations in the open air, thereby dramatically increasing the outward ion
9 transport capacity of the large-scale corona plasma discharge installation. As a result, the large ion
10 coverage area (30 m \times 23 m \times 90 m) has been achieved experimentally and validated by the numerical
11 calculations. The faster wind speed was a more efficient way to increase the ion coverage area. The
12 cloud chamber experiment confirms that the charged aerosols generated by ions can accelerate the
13 settlement of moisture by 38%. These results indicate that the large scale corona discharge
14 installation indeed can increase the ion density within a certain region. Furthermore, the ion-induced
15 charged aerosols may realistically trigger water precipitation or, alternatively, fog elimination. Since
16 the latter effects were studied using our large-scale cloud chamber laboratory system, systematic
17 field studies under real-world conditions are warranted to optimize the complex processes involved
18 in ion-induced precipitation of atmospheric aerosols under prevailing weather conditions.

19 *Data availability.* Data are available from the corresponding author upon a reasonable request.

20

21 *Author contributions.* SM and HC made equal contributions. DL initiated and supervised the study.
22 JL and MX performed experimental studies. DL and KO collaborated on interpreting the results. DL
23 prepared the manuscript, with significant contributions from HC, JL, and KO.

24

25 *Competing interests.* The authors declare that they have no conflict of interest.

26

27 *Acknowledgements.* This work was supported by the National Key Research and Development Plan
28 of China (Grant No.2016YFC0401001)

29



1

2

3 **References**

- 4 Albani, R. A. S. and Albani, V. V. L.: Tikhonov-type regularization and the finite element method applied to point source estimation in
5 the atmosphere, *Atmospheric Environment*, 211, 69–78, doi:10.1016/j.atmosenv.2019.04.063, 2019.
- 6 Albani, R. A. S., Duda, F. P. and Pimentel, L. C. G.: On the modeling of atmospheric pollutant dispersion during a diurnal cycle: A
7 finite element study, *Atmospheric Environment*, 118, 19–27, doi:10.1016/j.atmosenv.2015.07.036, 2015.
- 8 Anon: Estimation of the agglomeration coefficient of bipolar-charged aerosol particles, *Journal of Electrostatics*, 48(2), 93–101,
9 doi:10.1016/S0304-3886(99)00053-4, 2000.
- 10 Antao, D. S., Staack, D. A., Fridman, A. and Farouk, B.: Atmospheric pressure dc corona discharges: operating regimes and potential
11 applications, *Plasma Sources Sci. Technol.*, 18(3), 035016, doi:10.1088/0963-0252/18/3/035016, 2009.
- 12 Ashrafi, K., Orkomi, A. A. and Motlagh, M. S.: Direct effect of atmospheric turbulence on plume rise in a neutral atmosphere,
13 *Atmospheric Pollution Research*, 8(4), 640–651, doi:10.1016/j.apr.2017.01.001, 2017.
- 14 Bao, P., Lu, X., He, M. and Liu, D.: Kinetic Analysis of Delivery of Plasma Reactive Species Into Cells Immersed in Culture Media,
15 *IEEE Transactions on Plasma Science*, PP(99), 1–9, doi:10.1109/TPS.2016.2578955, 2016.
- 16 Bricard, J., Billard, F. and Madelaine, G.: Formation and evolution of nuclei of condensation that appear in air initially free of aerosols,
17 *Journal of Geophysical Research* (1896-1977), 73(14), 4487–4496, doi:10.1029/JB073i014p04487, 1968.
- 18 Carslaw, K. S., Harrison, R. G. and Kirkby, J.: Cosmic Rays, Clouds, and Climate, *Science*, 298(5599), 1732–1737,
19 doi:10.1126/science.1076964, 2002.
- 20 Chen, J. and Davidson, J. H.: Model of the Negative DC Corona Plasma: Comparison to the Positive DC Corona Plasma, *Plasma
21 Chemistry and Plasma Processing*, 23(1), 83–102, doi:10.1023/A:1022468803203, 2003.
- 22 Cherrier, G., Belut, E., Gerardin, F., Tanière, A. and Rimbert, N.: Aerosol particles scavenging by a droplet: Microphysical modeling in
23 the Greenfield gap, *Atmospheric Environment*, 166, 519–530, doi:10.1016/j.atmosenv.2017.07.052, 2017.
- 24 Dai, A.: Increasing drought under global warming in observations and models, *Nature Clim Change*, 3(1), 52–58,
25 doi:10.1038/nclimate1633, 2013.
- 26 Dawei Liu, Iza, F. and Kong, M. G.: Evolution of the Light Emission Profile in Radio-Frequency Atmospheric Pressure Glow
27 Discharges, *Plasma Science, IEEE Transactions on DOI - 10.1109/TPS.2008.922426*, 36(4), 952–953, 2008.
- 28 Farr, T. G. and Chadwick, O. A.: Geomorphic processes and remote sensing signatures of alluvial fans in the Kun Lun Mountains,
29 China, *Journal of Geophysical Research: Planets*, 23091–23100, doi:10.1029/96JE01603@10.1002/(ISSN)2169-9100.SIRSAR1,
30 2012.
- 31 Frederick, J. E. and Tinsley, B. A.: The response of longwave radiation at the South Pole to electrical and magnetic variations: Links to
32 meteorological generators and the solar wind, *J. Atmos. Sol.-Terr. Phys.*, 179, 214–224, doi:10.1016/j.jastp.2018.08.003, 2018.



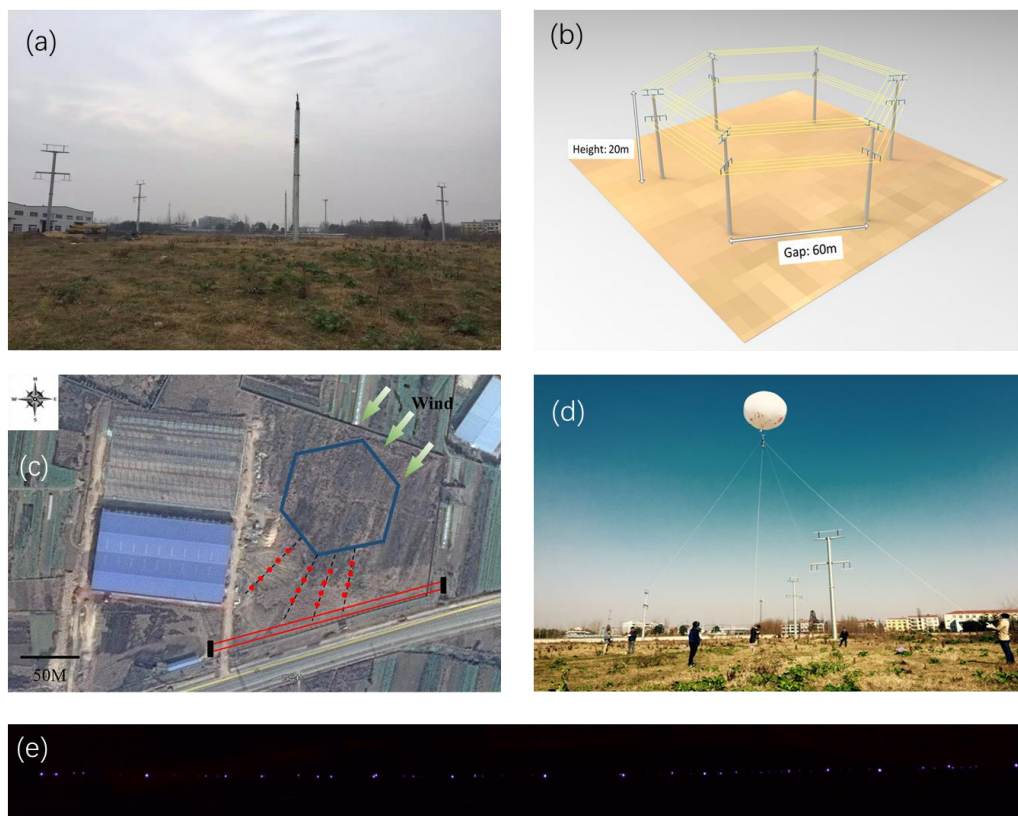
- 1 Gan, L., Duan, J., Zhang, S., Liu, X., Poorun, D., Liu, X., Lu, X., Duan, X., Liu, D. and Chen, H.: Cold atmospheric plasma
2 ameliorates imiquimod-induced psoriasiform dermatitis in mice by mediating antiproliferative effects, *Free Radical Research*, 53(3),
3 269–280, doi:10.1080/10715762.2018.1564920, 2019.
- 4 Harrison, R. G.: Cloud Formation and the Possible Significance of Charge for Atmospheric Condensation and Ice Nuclei, *Space*
5 *Science Reviews*, 94(1–2), 381–396, doi:10.1023/A:1026708415235, 2000.
- 6 Harrison, R. G. and Carslaw, K. S.: Ion-aerosol-cloud processes in the lower atmosphere, *Reviews of Geophysics*, 41(3),
7 doi:10.1029/2002RG000114, 2003.
- 8 Hashino, T., Chiruta, M., Polzin, D., Kubicek, A. and Wang, P. K.: Numerical simulation of the flow fields around falling ice crystals
9 with inclined orientation and the hydrodynamic torque, *Atmospheric Research*, 150, 79–96, doi:10.1016/j.atmosres.2014.07.003, 2014.
- 10 He, J., Hu, J., Liu, D. and Zhang, Y.-T.: Experimental and numerical study on the optimization of pulse-modulated radio-frequency
11 discharges, *Plasma Sources Sci. Technol.*, 22(3), 035008, doi:10.1088/0963-0252/22/3/035008, 2013.
- 12 Henin, S., Petit, Y., Kiselev, D., Kasparian, J. and Wolf, J.-P.: Contribution of water droplets to charge release by laser filaments in air,
13 *Appl. Phys. Lett.*, 95(9), 091107, doi:10.1063/1.3220066, 2009.
- 14 Hosseini, B. and Stockie, J. M.: Bayesian estimation of airborne fugitive emissions using a Gaussian plume model, *Atmospheric*
15 *Environment*, 141, 122–138, doi:10.1016/j.atmosenv.2016.06.046, 2016.
- 16 Hu, J. T., Liu, X. Y., Liu, J. H., Xiong, Z. L., Liu, D. W., Lu, X. P., Iza, F. and Kong, M. G.: The effect of applied electric field on
17 pulsed radio frequency and pulsed direct current plasma jet array, *Physics of Plasmas*, 19(6), 063505-063505–5,
18 doi:10.1063/1.4729730, 2012.
- 19 Hu, J. T., Wang, J. G., Liu, X. Y., Liu, D. W., Lu, X. P., Shi, J. J. and Ostrikov, K.: Effect of a floating electrode on a plasma jet,
20 *Physics of Plasmas*, 20(8), 083516-083516–5, doi:10.1063/1.4817954, 2013.
- 21 Jidenko, N. and Borra, J. P.: Self-cleaning, maintenance-free aerosol filter by non-thermal plasma at atmospheric pressure, *Journal of*
22 *Hazardous Materials*, 235–236, 237–245, doi:10.1016/j.jhazmat.2012.07.055, 2012.
- 23 Jolly, W. M., Cochrane, M. A., Freeborn, P. H., Holden, Z. A., Brown, T. J., Williamson, G. J. and Bowman, D. M. J. S.:
24 Climate-induced variations in global wildfire danger from 1979 to 2013, *Nat Commun*, 6(1), 1–11, doi:10.1038/ncomms8537, 2015.
- 25 Keefe, D., Nolan, P. J. and Rich, T. A.: Charge Equilibrium in Aerosols According to the Boltzmann Law, *Proceedings of the Royal*
26 *Irish Academy. Section A: Mathematical and Physical Sciences*, 60, 27–45, 1959.
- 27 Khain, A., Arkhipov, V., Pinsky, M., Feldman, Y. and Ryabov, Y.: Rain enhancement and fog elimination by seeding with charged
28 droplets. part I: Theory and numerical simulations, *J. Appl. Meteorol.*, 43(10), 1513–1529, doi:10.1175/JAM2131.1, 2004.
- 29 Lesk, C., Rowhani, P. and Ramankutty, N.: Influence of extreme weather disasters on global crop production, *Nature*, 529(7584),
30 84–87, doi:10.1038/nature16467, 2016.
- 31 Liu, J. H., Liu, X. Y., Hu, K., Liu, D. W., Lu, X. P., Iza, F. and Kong, M. G.: Plasma plume propagation characteristics of pulsed radio
32 frequency plasma jet, *Applied Physics Letters*, 98, 151502, doi:10.1063/1.3573811, 2011.
- 33 Liu, X., Gan, L., Ma, M., Zhang, S., Liu, J., Chen, H., Liu, D. and Lu, X.: A comparative study on the transdermal penetration effect of
34 gaseous and aqueous plasma reactive species, *J. Phys. D: Appl. Phys.*, 51(7), 075401, doi:10.1088/1361-6463/aaa419, 2018.



- 1 Liu, X. Y., Hu, J. T., Liu, J. H., Xiong, Z. L., Liu, D. W., Lu, X. P. and Shi, J. J.: The discharge mode transition and O(5p1) production
2 mechanism of pulsed radio frequency capacitively coupled plasma, *Applied Physics Letters*, 101(4), 043705-043705-4,
3 doi:doi:10.1063/1.4733662, 2012.
- 4 Liu, X. Y., Pei, X. K., Lu, X. P. and Liu, D. W.: Numerical and experimental study on a pulsed-dc plasma jet, *Plasma Sources Sci.*
5 *Technol.*, 23(3), 035007, doi:10.1088/0963-0252/23/3/035007, 2014a.
- 6 Liu, X. Y., Pei, X. K., Ostrikov, K., Lu, X. P. and Liu, D. W.: The production mechanisms of OH radicals in a pulsed direct current
7 plasma jet, *Physics of Plasmas* (1994-present), 21(9), 093513, doi:10.1063/1.4895496, 2014b.
- 8 Luan, T., Guo, X., Zhang, T. and Guo, L.: Below-Cloud Aerosol Scavenging by Different-Intensity Rains in Beijing City, *J Meteorol*
9 *Res*, 33(1), 126–137, doi:10.1007/s13351-019-8079-0, 2019.
- 10 Mu, Y., Pang, X., Quan, J. and Zhang, X.: Atmospheric carbonyl compounds in Chinese background area: A remote mountain of the
11 Qinghai-Tibetan Plateau, *Journal of Geophysical Research: Atmospheres*, 112(D22), doi:10.1029/2006JD008211, 2007.
- 12 Nielsen, J., Maus, C., Rzesanke, D. and Leisner, T.: Charge induced stability of water droplets in subsaturated environment,
13 *Atmospheric Chemistry and Physics*, 11, doi:10.5194/acp-11-2031-2011, 2011.
- 14 Pan, S., Xu, M., Gan, L., Zhang, S., Chen, H., Liu, D., Li, Y. and Lu, X.: Plasma activated radix arnebiae oil as innovative
15 antimicrobial and burn wound healing agent, *J. Phys. D: Appl. Phys.*, 52(33), 335201, doi:10.1088/1361-6463/ab234c, 2019.
- 16 Pierce, J. R. and Adams, P. J.: Can cosmic rays affect cloud condensation nuclei by altering new particle formation rates?, *Geophysical*
17 *Research Letters*, 36(9), doi:10.1029/2009GL037946, 2009.
- 18 Riba, J.-R., Morosini, A. and Capelli, F.: Comparative Study of AC and Positive and Negative DC Visual Corona for Sphere-Plane
19 Gaps in Atmospheric Air, *Energies*, 11(10), 2671, doi:10.3390/en11102671, 2018.
- 20 Roy, A., Chatterjee, A., Ghosh, A., Das, S. K., Ghosh, S. K. and Raha, S.: Below-cloud scavenging of size-segregated aerosols and its
21 effect on rainwater acidity and nutrient deposition: A long-term (2009-2018) and real-time observation over eastern Himalaya, *Sci.*
22 *Total Environ.*, 674, 223–233, doi:10.1016/j.scitotenv.2019.04.165, 2019.
- 23 Schleder, A. M. and Martins, M. R.: Experimental data and CFD performance for CO₂ cloud dispersion analysis, *Journal of Loss*
24 *Prevention in the Process Industries*, 43, 688–699, doi:10.1016/j.jlp.2016.03.027, 2016.
- 25 Shiyin, L., Wenxin, S., Yongping, S. and Gang, L.: Glacier changes since the Little Ice Age maximum in the western Qilian Shan,
26 northwest China, and consequences of glacier runoff for water supply, *Journal of Glaciology*, 49(164), 117–124,
27 doi:10.3189/172756503781830926, 2003.
- 28 Tan, X., Qiu, Y., Yang, Y., Liu, D., Lu, X. and Pan, Y.: Enhanced Growth of Single Droplet by Control of Equivalent Charge on
29 Droplet, *IEEE Transactions on Plasma Science*, PP(99), 1–5, doi:10.1109/TPS.2016.2608832, 2016.
- 30 Tinsley, B. A. and Zhou, L.: Parameterization of aerosol scavenging due to atmospheric ionization, *J. Geophys. Res.-Atmos.*, 120(16),
31 8389–8410, doi:10.1002/2014JD023016, 2015.
- 32 Trenberth, K. E., Dai, A., Schrier, G. van der, Jones, P. D., Barichivich, J., Briffa, K. R. and Sheffield, J.: Global warming and changes
33 in drought, *Nature Clim Change*, 4(1), 17–22, doi:10.1038/nclimate2067, 2014.
- 34 Wang, J. G., Liu, X. Y., Liu, D. W., Lu, X. P. and Zhang, Y. T.: Mathematical model of gas plasma applied to chronic wounds, *Physics*



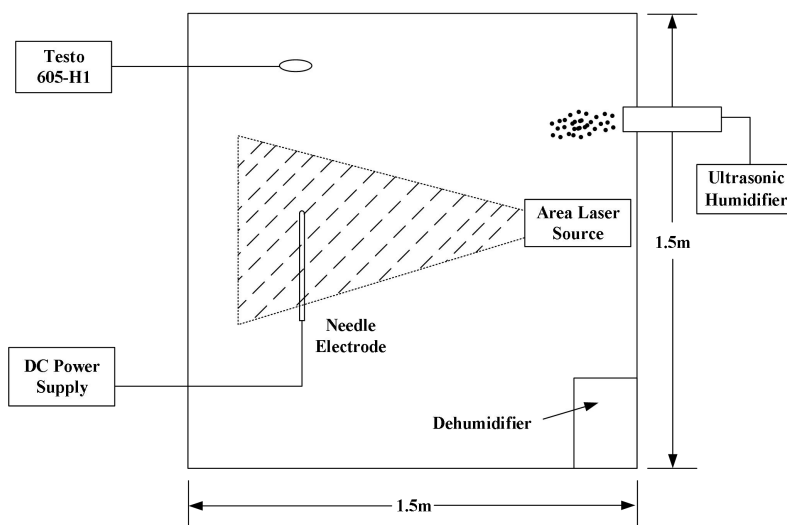
- 1 of Plasmas (1994-present), 20(11), 113507, doi:10.1063/1.4826955, 2013.
- 2 Wang, P. K. and Pruppacher, H. R.: An Experimental Determination of the Efficiency with Which Aerosol Particles are Collected by
3 Water Drops in Subsaturated Air, *J. Atmos. Sci.*, 34(10), 1664–1669, doi:10.1175/1520-0469(1977)034<1664:AEDOTE>2.0.CO;2,
4 1977.
- 5 Yang, Y., Tan, X., Liu, D., Lu, X., Zhao, C., Lu, J. and Pan, Y.: Corona Discharge-Induced Rain and Snow Formation in Air, *IEEE*
6 *Trans. Plasma Sci.*, 46(5), 1786–1792, doi:10.1109/TPS.2018.2820200, 2018.
- 7 Yao, X., Jiang, N., Li, J., Lu, N., Shang, K. and Wu, Y.: An improved corona discharge ignited by oxide cathodes with high secondary
8 electron emission for toluene degradation, *Chem. Eng. J.*, 362, 339–348, doi:10.1016/j.cej.2018.12.151, 2019.
- 9 Zhang, B., He, J. and Ji, Y.: Prediction of average mobility of ions from corona discharge in air with respect to pressure, humidity and
10 temperature, *IEEE Trns. Dielectr. Electr. Insul.*, 26(5), 1403–1410, doi:10.1109/TDEI.2019.008001, 2019.
- 11 Zhang, L. and Tinsley, B. A.: Parameterization of aerosol scavenging due to atmospheric ionization under varying relative humidity, *J.*
12 *Geophys. Res.-Atmos.*, 122(10), 5330–5350, doi:10.1002/2016JD026255, 2017.
- 13 Zhang, L., Tinsley, B. A. and Zhou, L.: Parameterization of In-Cloud Aerosol Scavenging Due to Atmospheric Ionization: Part 3.
14 Effects of Varying Droplet Radius, *J. Geophys. Res.-Atmos.*, 123(18), 10546–10567, doi:10.1029/2018JD028840, 2018a.
- 15 Zhang, L., Tinsley, B. A. and Zhou, L.: Parameterization of In-Cloud Aerosol Scavenging Due to Atmospheric Ionization: Part 3.
16 Effects of Varying Droplet Radius, *J. Geophys. Res.-Atmos.*, 123(18), 10546–10567, doi:10.1029/2018JD028840, 2018b.
- 17 Zhou, X. and Yang, J.: A Novel Solar Thermal Power Plant with Floating Chimney Stiffened onto a Mountainside and Potential of the
18 Power Generation in China's Deserts, *Heat Transfer Engineering*, doi:10.1080/01457630802414813, 2010.
- 19 Zou, X., Xu, M., Pan, S., Gan, L., Zhang, S., Chen, H., Liu, D., Lu, X. and Ostrikov, K. K.: Plasma Activated Oil: Fast Production,
20 Reactivity, Stability, and Wound Healing Application, *ACS Biomater. Sci. Eng.*, 5(3), 1611–1622,
21 doi:10.1021/acsbomaterials.9b00125, 2019.
- 22
- 23
- 24
- 25



1

2 **Figure 1.** Large-scale installation for ion generation for precipitation of atmospheric aerosols, using
3 over 300,000 corona plasma discharges. (a) The large-scale corona discharge system consists of 6
4 poles and 7.2 km electric wires. (b) The design diagram of the hexagonal discharge arrays. (c) The
5 satellite image of the test zone (taken from <https://map.baidu.com>, last access: 29 December 2019).
6 The hexagon shows the corona plasma discharge system. The red points show the locations of ion
7 density measurements. (d) The hydrogen balloon carried the ion density measurement device. (e) The
8 image of corona discharge on the wire (1 m length, -40 kV). The exposure time of the image is 0.5
9 seconds. The wire (diameter of 1 mm) was six strands of stranded wire.

10



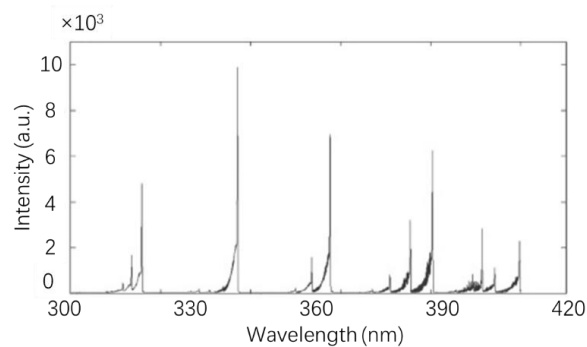
1

2

3 **Figure 2.** Schematic of the 6.75m³ cloud chamber used for the ion-enhanced precipitation.

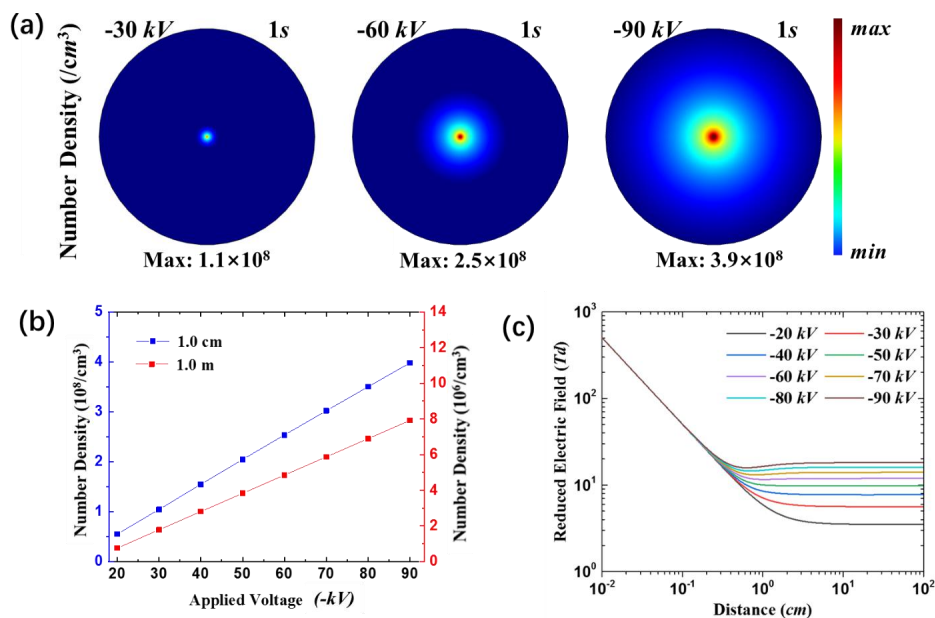
4

5



6

7 **Figure 3.** Nitrogen species dominate the optical emission spectra (shown between 300 nm and 400
8 nm here) from the negative corona discharge on the wire electrode generated with the applied voltage
9 of -40 kV.



1

2

3 **Figure 4.** The increasing applied voltage enhances the ion output capacity of the corona discharge
4 source. (a) The distribution of ions generated by single corona discharge point (simulation). The
5 center is the corona discharge point. The radius of the big blue circle is 1 m. (b) The ion density at 1
6 cm from the center as a function of applied voltage. (c) The electric field from the center as a
7 function of applied voltage.

8

9

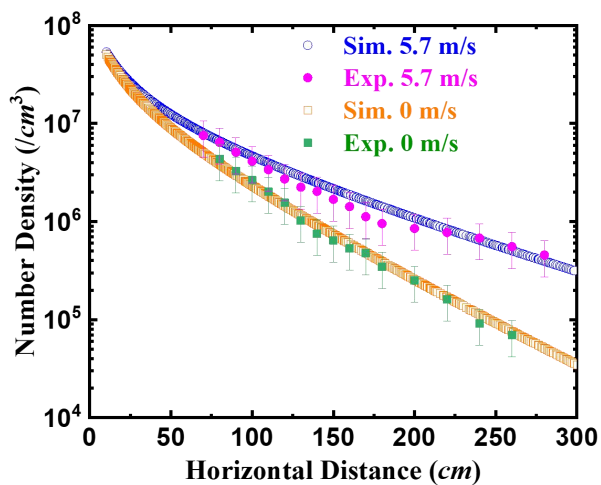
10

11

12



1



2

3 **Figure 5.** The effect of wind on the distribution of ions generated by a single corona discharge point
4 (indoor tests). Wind speed at 0 m/s and 5.7 m/s. The applied voltage on the wire electrode was -40
5 kV. The experiment measurement data is plotted with error bar. The simulation data is plotted by
6 hollow symbols.

7

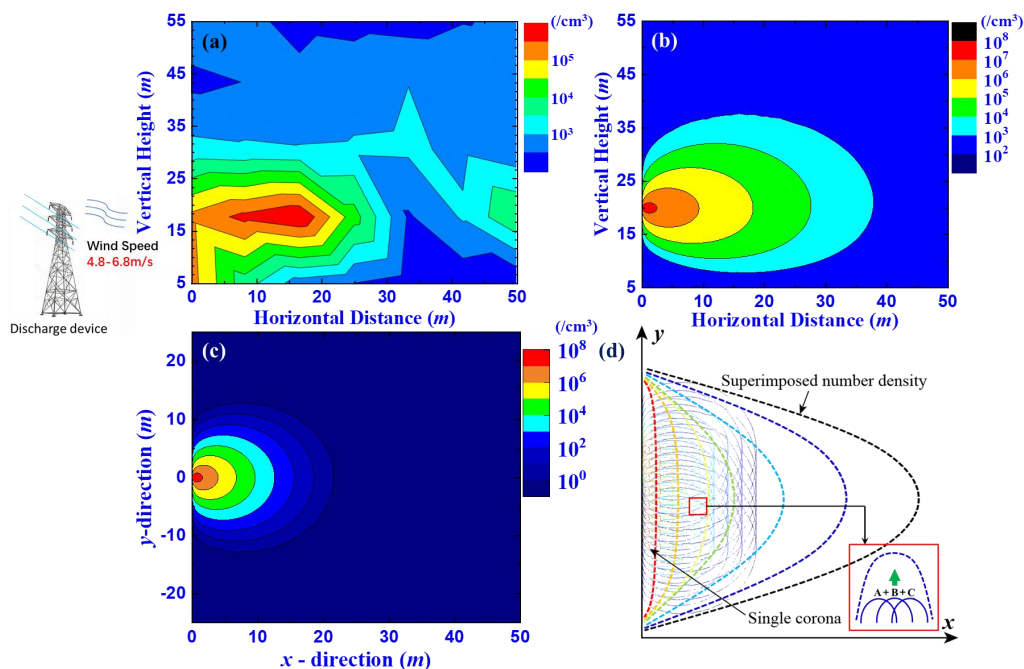
8

9

10

11

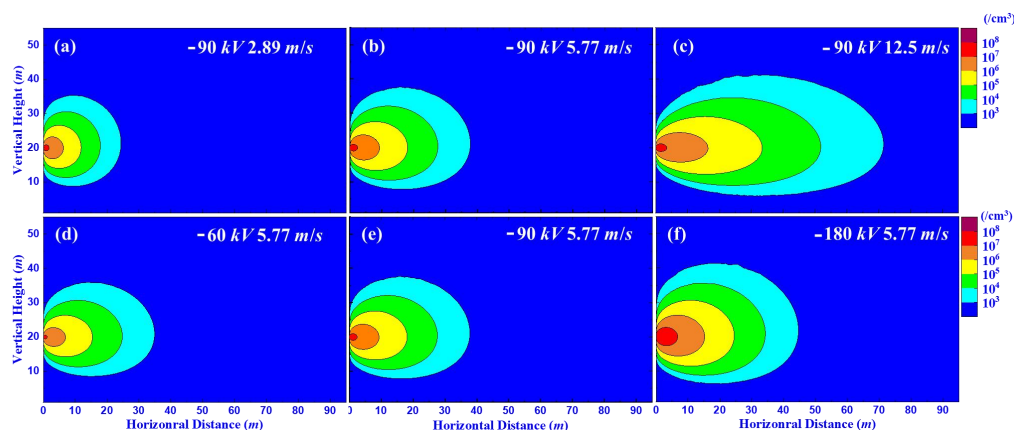
12



1

2 **Figure 6.** The coverage area of the large corona discharge system is the combination of the coverage
3 areas of the very large number of corona discharge points. (a) The ion density distribution in vertical
4 direction and downwind direction (experimental measurement, applied voltage -90 kV). (b) The ion
5 density distribution in vertical direction and downwind direction (simulation, z axis (vertical
6 direction), x axis (horizontal direction)). (c) The ion density distribution of single corona discharge
7 point (-90 kV) in horizontal direction (x-y axis). (d) The combination of ions generated by multi-
8 corona discharge points resulted in high negative ion density in the open air. The dashed color lines
9 from red color to black color suggests the ion density decreases as the distance from the wire
10 electrode increases. The inserted picture indicates the combination of ions generated by three corona
11 discharge sources increases the coverage of ions substantially.

12



1

2

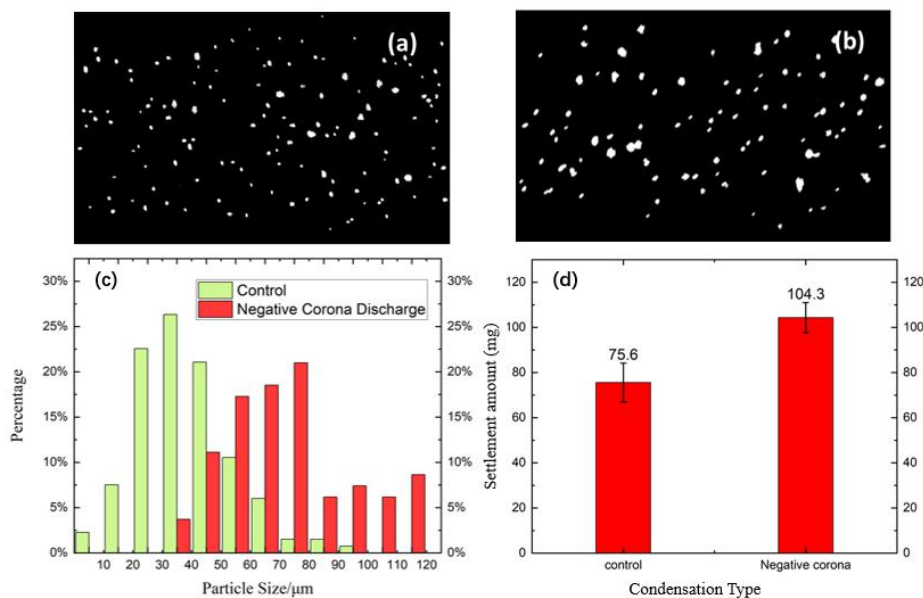
3 **Figure 7.** The increasing applied voltage and wind speed can enlarge the coverage area of the ion
4 source. The effect of wind on the ion distribution in the field (numerical results). (a) -90kV, 2.89m/s
5 (wind speed), (b)-90kV, 5.77m/s, (c)-90 kV, 12.5 m/s. The effect of wind on the ion distribution in
6 the field (numerical results). (d) -60 kV. (e) -90 kV. (f) -180 kV.

7

8



1



2

3 **Figure 8.** The ions generated by corona discharge source enhance the condensation of aerosols. The
4 photo of aerosols in the light path of a laser for the case of (a) control group, (b) the enhanced
5 condensation group by ions. The photo was taken 5 min after the experiment started. (c)The particle
6 size distribution of aerosols in the cloud chamber for the control group and negative corona discharge
7 group (calculated according to (a) and (b)). (d) The ions generated by corona discharge source
8 enhance settlement of moisture. The settlement of moisture of control, negative corona discharge
9 groups on the acceptor 10 min after the experiment started.

10